ELSEVIER

Tectonophysics 333 (2001) 219–240

TECTONOPHYSICS

www.elsevier.com/locate/tecto

# Continuous monitoring of an active fault in a plate suture zone: a creepmeter study of the Chihshang Fault, eastern Taiwan

J.-C. Lee[a,*], J. Angelier[b], H.-T. Chu[c], J.-C. Hu[d], F.-S. Jeng[e]

[a]*Institute of Earth Sciences, Academia Sinica, P.O. Box 1-55, Nankang, Taipei 115, Taiwan, ROC*
[b]*Tectonique Quantitative, Département de Géotectonique and ESA 7072, Université P.-&-M. Curie, Paris, France*
[c]*Central Geological Survey, P.O. Box 968, Taipei, Taiwan, ROC*
[d]*The Institute for Secondary School Teacher of Taiwan, Taichung, Taiwan, ROC*
[e]*Department of Civil Engineering, National Taiwan University, Taipei, Taiwan, ROC*

**Abstract**

Data from continuously monitored creepmeters across the active Chihshang Fault in eastern Taiwan are presented. The Chihshang Fault is an active segment of the Longitudinal Valley Fault, the main suture between the converging Philippine and Eurasian plates in Taiwan. Since the 1951 earthquake (Mw = 7.0), no earthquake larger than magnitude 6.0 occurred in the Chihshang area. At least during the last 20 years, the Chihshang Fault underwent a steady creep movement, resulting in numerous fractures at the surface. Five creepmeters were installed in 1998 at two sites, Tapo and Chinyuan, within the Chihshang active fault zone. One-year results (from August 1998 to July 1999) show a horizontal shortening of 19.4 ± 0.3 mm and 17.3 ± 0.7 mm, at Tapo and Chinyuan, respectively. These annual shortening rates are in a good agreement with other estimates of strain rate independently obtained from geodetic measurements and geological site investigation. The creepmeter measurements were made on a daily basis, providing accurate information on the previously unknown evolution of creep during the year. The records of fault creep at the Tapo site thus revealed close seasonal correlation with average rainfall: the period of high creep rate coincides with the wet season, whereas that of low creep rate coincides with the dry season. Also, in comparison with the Tapo site, the creep behaviour as a function of time is complex at the Chinyuan site. Possible factors of irregularity are under investigation (thermal effect acting on the concrete basement of the creepmeters, earth tide effect, water table variations in a nearby rice field, and rainfall). The comparison between GPS measurements across the Longitudinal Valley (31 mm/year of horizontal displacement) and the creepmeter measurement across the Chihshang Fault zone (17–19 mm/year of horizontal displacement) suggests that there exists other shortening deformation across the active fault zone in addition to those we have measured from the creepmeters. 

*Keywords*: creepmeter; active fault; fault creep; plate suture

## 1. Introduction

The Longitudinal Valley in eastern Taiwan is the present-day suture zone between the Philippine Sea plate and the Eurasian plate (Fig. 1a). Based on recent GPS studies (Yu et al., 1997), the oblique convergence of these two plates occurs in the NW–SE direction across the Taiwan mountain belt at a shortening rate of 85 mm/year. Results of the analysis of the geodetic trilateration network (Yu et al., 1990; Lee and Angelier, 1993; Lee et al., 1998) and geological site investigation (Lee, 1994; Angelier et al., 1997,

* Corresponding author. Tel.: +886-2-27839910, ext. 409; fax: +886-2-2783-9871.
*E-mail address:* jclee@earth.sinica.edu.tw (J.-C. Lee).

0040-1951/00/$ - see front matter 
PII: S0040-1951(00)00276-6

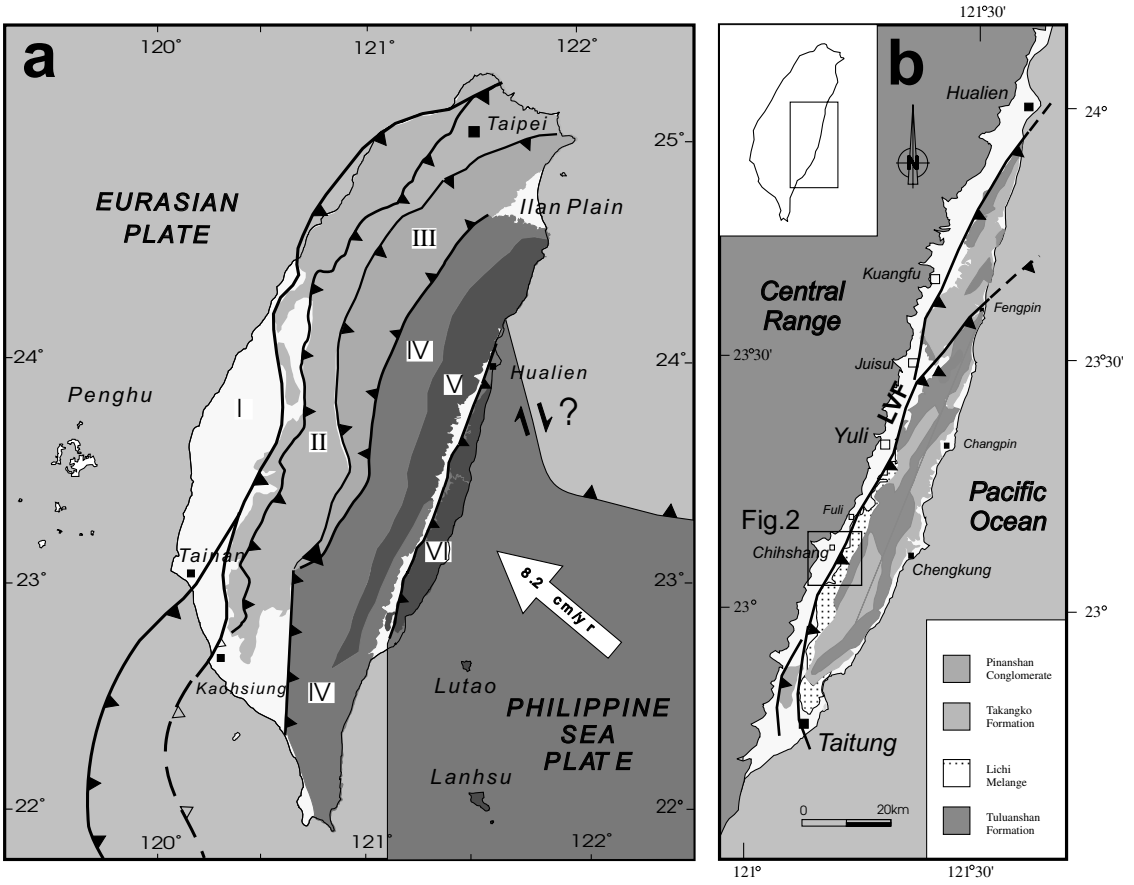


Fig. 1. (a) General geology and tectonic setting of Taiwan. Rock units I–V belong to the Eurasian plate: I, Coastal plain; II, Foothills; III, Hsuehshang Range; IV, Backbone Range; V, Tananao metamorphic basement. Rock unit VI, Coastal Range, belongs to the Philippine Sea plate. (b) General geology of the Coastal Range. The Coastal Range overthrusted onto the Longitudinal valley and the Central Range along the active Longitudinal Valley Fault (LVF, heavy line with triangles).

1999) indicated that the Longitudinal Valley Fault (LVF) absorbed about one fourth (20–25 mm/year) of the total plate convergence (Fig. 1b).

The active Chihshang Fault, located in the middle part of the Longitudinal Valley (Fig. 1b), is one of the most active segments of the LVF (Yu et al., 1990). This active fault accommodates left-lateral westward thrusting of the Coastal Range, a northern extension of the Luzon arc system of the Philippine Sea plate, onto the Longitudinal Valley and the Central Range (belonging to the Eurasian plate). From the seismological point of view, no significant earthquake (Magnitude $\geq 6.0$) has occurred in the Chihshang area since the 1951 'Taitung earthquakes' (Mw = 7.0 and 6.2). During the last 20 years, the Chihshang Fault has moved gradually by creeping, without abrupt seismic slip (Yu and Liu, 1989; Angelier et al., 1999). The fault creep left numerous fractures in concrete water channels, walls, houses, etc. In some situations, these surface features allowed qualitative and quantitative characterization of active creep at the Chihshang Fault (Angelier et al., 1997, 1999). In a further attempt to continuously monitor surface crustal deformation in the active fault zone, we have recently installed five rod-type creepmeters (strainmeters) in the Chihshang Fault zone.

The aim of this paper is to monitor the displacement of the active Chihshang Fault and to characterize the creep behaviour, based on a creepmeter study. In this paper, we first briefly describe the geological

characteristics of the Chihshang active fault. We then present the instrumentation involving newly built rod-type creepmeters and show the results of the continuous monitoring of the displacement of the Chihshang Fault based on the new data thus obtained. We finally discuss the implications of the results and the factors that control the fault creep.

## 2. The Chihshang active fault

### 2.1. Tectonic and geological setting

The Chihshang Fault belongs to a portion of the southern segment of the LVF. The Longitudinal Valley, situated in eastern Taiwan (Fig. 1b), is the main suture of present-day convergence between the Philippine Sea plate and the Eurasian plate. The LVF is a major active boundary fault (e.g. Tsai, 1986), the Coastal Range of the Philippine Sea plate being thrusted westward over the Longitudinal Valley and the Central Range of the Eurasian plate.

The Coastal Range of the Luzon island-arc system (Fig. 2) is composed of the Miocene andesitic volcanic basement (Tuluanshan Formation), the Pliocene Lichi Mélange, and overlying Plio-Pleistocene flysch-type deposits of the Takangkou Formation (Hsu, 1956, 1976; Teng and Wang, 1981; Page and Suppe, 1981). The metamorphic terranes of the pre-Neogene continental margin crops out in the Central Range, west of the Longitudinal Valley. In the Chihshang area, the eastern edge of the Central Range consists principally of highly deformed low grade Paleogene slate (or phyllite) and quartz–feldspars metasandstone of the Hsinkao Formation (Stanley et al., 1981). Between the Central Range and the Coastal Range, the suture of the Longitudinal Valley is covered by Quaternary alluvial deposits.

Morphologically, several features reveal active faulting in the Chihshang area (Fig. 2). The active Chihshang Fault is located in front of a topographic high within the Longitudinal Valley (Lee, 1994; Angelier et al., 1997). In the Longitudinal Valley, a major water-divide, with a huge alluvial fan on the western side (Fig. 2), is closely related to the compressional deformation that concentrated in the Chihshang area during the late Quaternary. A large pond in front of the active Chihshang Fault (Chihshang means ‘on

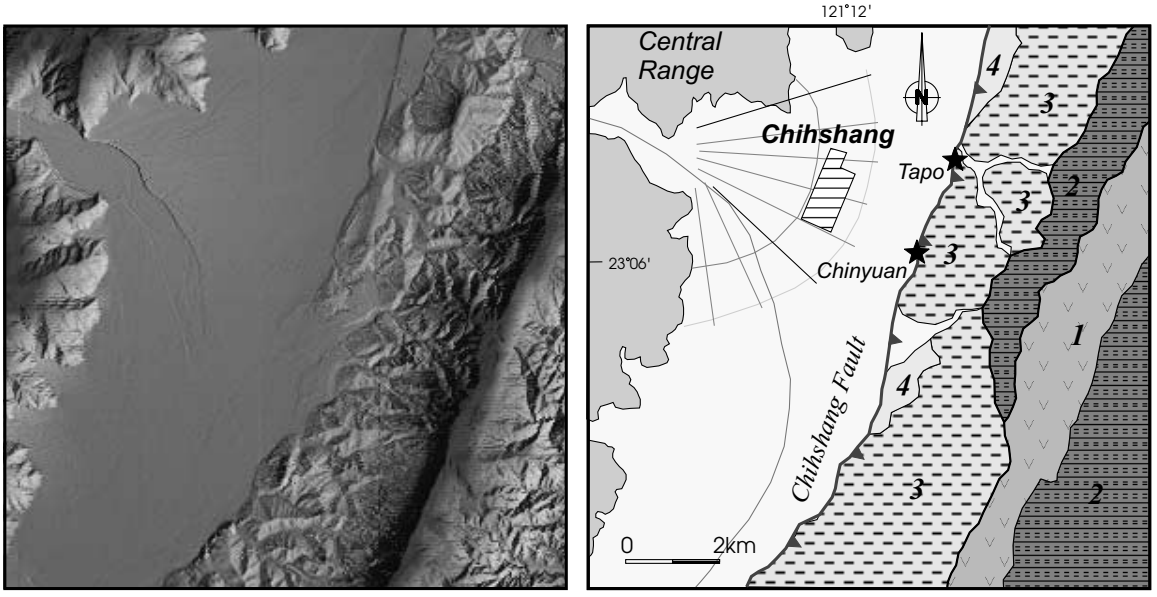


Fig. 2. General morphologic features and geology of the active Chihshang Fault. Left side: the digital elevation model’s (DEM) shading image. Right side: geological interpretation of the DEM. Geological units of the Coastal Range: 1, Touluanshan Formation; 2, Takangkou Formation; 3, Lichi Mélange; 4, Quaternary terrace. The Chihshang Fault is situated on the western margin of the Coastal Range. The two stars indicate the sites of creepmeters.

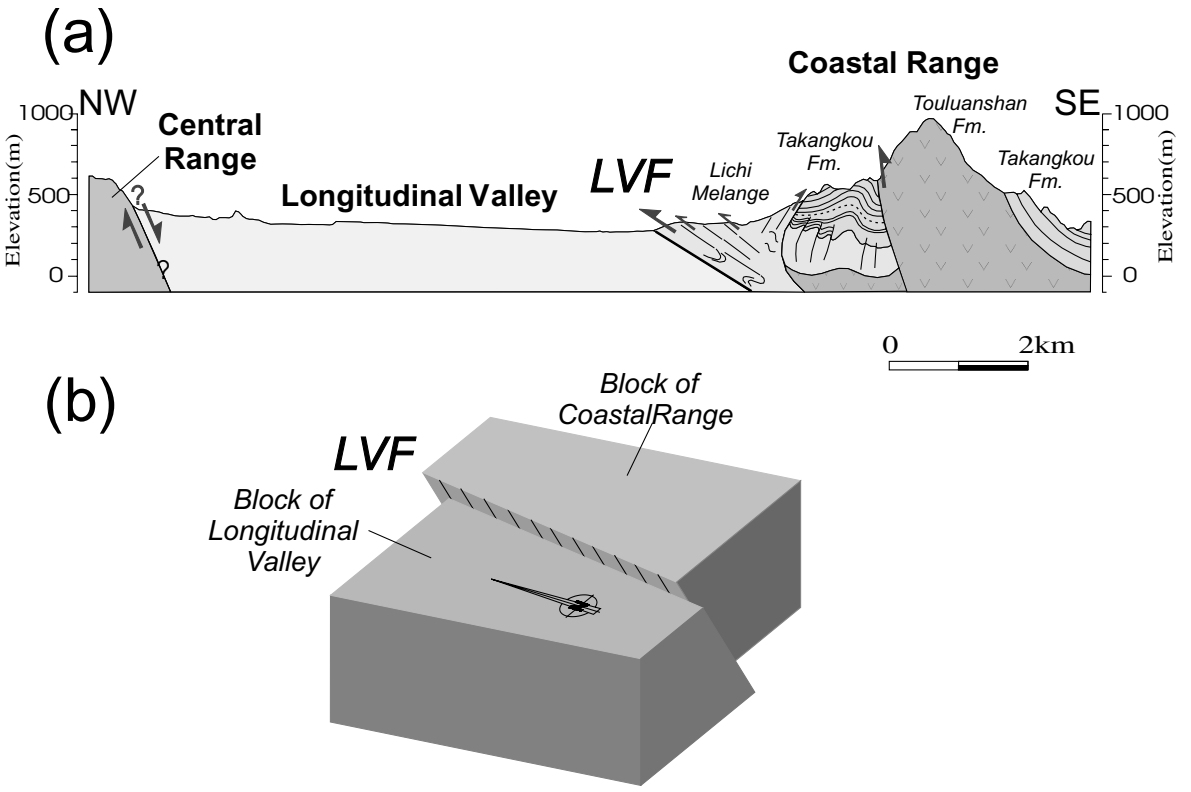


Fig. 3. (a) General cross-section of the Longitudinal Valley. The Coastal Range along the Longitudinal Valley Fault (LVF) overthrusts to the Longitudinal Valley. (b) 3D schematic reconstruction of the Longitudinal Valley Fault.

the pond' in Chinese) resulted from the bending of the footwall of the Chihshang active fault.

The Chihshang Fault strikes approximately N20°E and is at least 30-km long from Yuli (to the north) to Kuanshan (to the south). The fault zone crops out at the foot of the hills of the Coastal Range. The hanging wall rock unit of the Chihshang Fault is constituted by the Lichi Mélange of the Coastal Range. The footwall of the Chihshang Fault is composed of Quaternary alluvium deposits of the Longitudinal Valley (Fig. 3a). An outcrop in Fuli, a few kilometers north of Chihshang, shows the westward thrust of the Lichi Mélange over Quaternary terrace deposits (Barrier and Chu, 1984; Angelier et al., 1999). The fault is reverse and exhibits an eastward dip of 45–55° (Fig. 3b).

### 2.2. Historical earthquakes and surface ruptures

The Taitung earthquakes ($Mw = 7.0$ and 6.2) occurred on November 25 (local time), 1951, and caused damage in the Taitung region including the Chihshang area. The 1951 Taitung earthquake was caused by the rupture of the LVF (Fig. 4). Surface rupture on the Chihshang Fault during the 1951 earthquakes revealed a general thrust scrap with left-lateral movement (TWB, 1952; Hsu, 1955, 1962; Cheng et al., 1996). Since that time, no significant earthquake (i.e. $M \geq 6$) has occurred in the Chihshang area. However, numerous episodes of microseismic activity have occurred in the Chihshang area and they have been recorded by the Central Weather Bureau (CWB) seismic network of Taiwan (Fig. 4).

Movement on the Chihshang Fault during the last 20 years has left numerous fractures on the surface. Near Chihshang, several fractures in walls, roads, and buildings have been observed along the active fault zone (Barrier and Chu, 1984; Chu et al., 1994; Lee, 1994). The development of most these fractures resulted from the creeping behaviour of the active

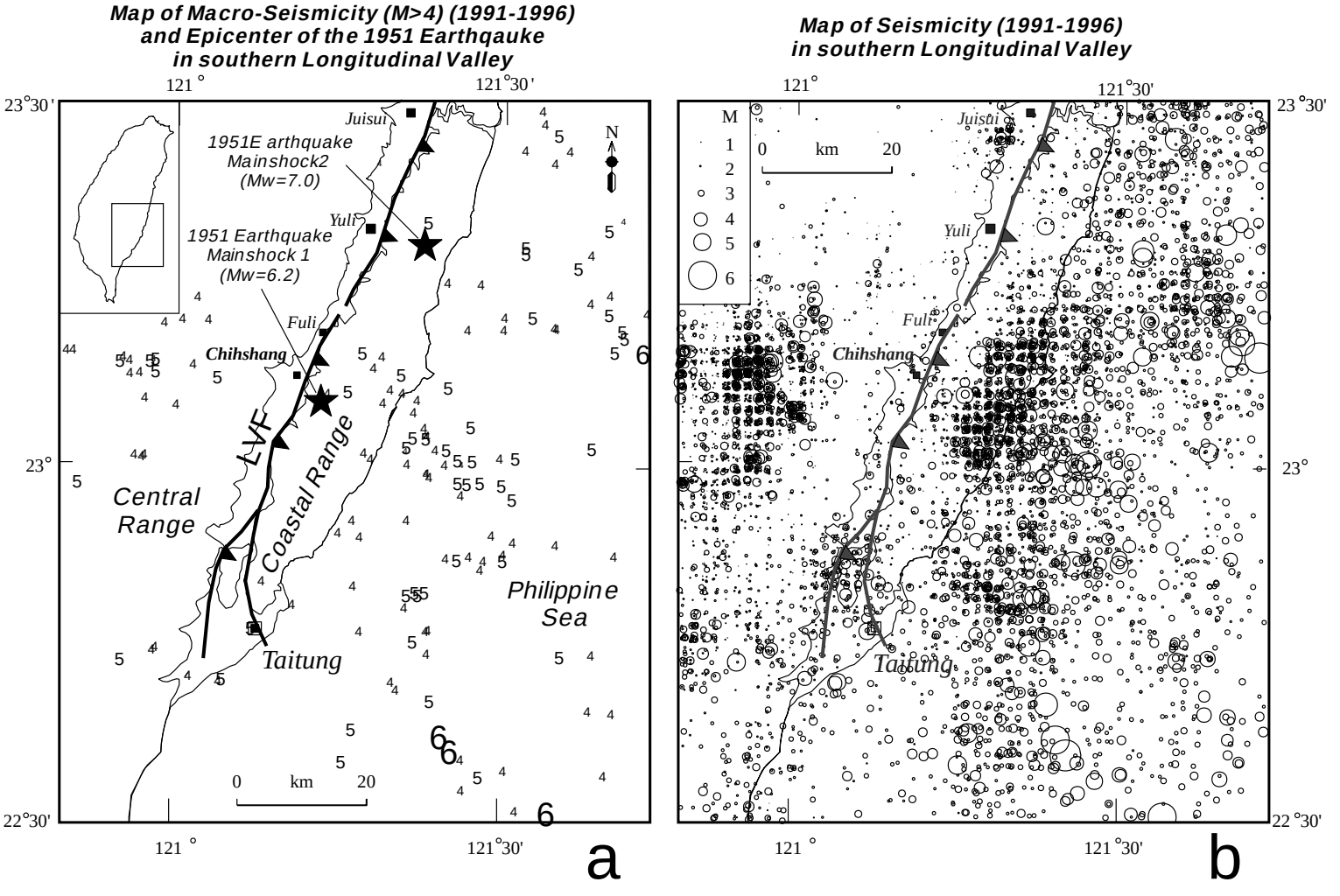


Fig. 4. Map of seismicity in the southern Longitudinal Valley. (a) Map of the macroseismicity ($M \geq 4$) from 1991 to 1996. The location of the mainshocks of the 1951 earthquake (Cheng et al., 1996), which resulted from the Longitudinal Valley Fault (LVF, heavy lines with triangles showing the overthrusted side), is marked by stars. (b) Map of all the seismicity recorded by the CWB network from 1991 to 1996. Note that there are numerous microseismicities but no earthquake larger than magnitude 6 in the Chihshang Fault area since the 1951 Mw = 7 earthquake.

fault, according to repeated field investigation (Angelier et al., 1997). Although the annual measurements along the active fault yielded reliable average creep velocities, no datum was available prior to the present study at a finer temporal resolution.

### 2.3. Measurements and estimates of fault movement

Recent movements of the Chihshang Fault have been documented by different techniques during the last 15 years, including geodetic studies (trilateration networks, levelling and GPS measurements: Yu and Liu, 1989; Lee and Angelier, 1993; Yu et al., 1997), geological and surface investigation (Chu et al., 1994; Lee, 1994; Angelier et al., 1997, 1999), micro-earthquake analysis (such as for the Yuli earthquakes: Yu and Tsai, 1982; Barrier and Angelier, 1986), and seismic and ground penetration radar profiling (Chow et al., 2001).

The 3D general displacement pattern of the Chihshang Fault was reconstructed by Lee and Angelier (1993) and Angelier et al. (1999), based on consideration of both the geological structure and available geodetic trilateration and levelling data. Based on a rigid-block model, the calculated horizontal displacement along the Chihshang Fault (Fig. 3b) shows a vector in the direction of N326°E (N34°W) with a velocity of 21 mm/year (Lee and Angelier, 1993). As a consequence, the movement of the Chihshang Fault includes a transverse (west-vergent thrust) component of 16.5 mm/year, a strike–slip (left-lateral) component of 13 mm/year, and a vertical (eastern uplift) component of 13 mm/year.

At the outcrop scale, the shortening rate of the Chihshang active fault has been estimated by detailed site studies along this active fault segment (Angelier et al., 1997, 1999). Annual surveys during the period 1991–1997 showed that the Chihshang Fault left several remarkable shortening deformation features at the surface and revealed a general constant slip rate of about 22 mm/year in the horizontal plane.

To more accurately measure the displacement with time, based on earlier detailed site investigation, we designed a creepmeter straddling the surface traces of the active fault to monitor the fault creep. The data from the creepmeter were expected to allow better understanding of the characteristics of active faulting and fault creep. We aimed at elucidating variation in fault displacement. Such variations could not be detected with the annual frequency of the earlier surveys. However, they became obvious during the latest period, when surveys were done twice a year and revealed significant changes so that the hypothesis of a rigorous steady-state slip suggested by the earlier surveys became no longer acceptable except as a first approximation (Angelier et al., 1997, 1999). Our interest in monitoring the displacement in a more continuous way thus arose. Another important reason to undertake this study lies on the relationships between changes in creep velocity and variations in the earthquake hazard. Although these relationships are still under study, an anomalous low creep rate of the active fault would be a possible indication of the lock of the fault movement (Schulz et al., 1982). The probability of the accumulation of stress within the crust and hence of occurrence of a large earthquake would thus increase, which highlights the importance of fault displacement monitoring.

## 3. Setting up of creepmeters: technical aspects

Creepmeters are common instruments (typically a wire or rod extensometer of 5–20-m length) for periodic or continuous measurement of fault creep (Smith and Wyss, 1968; Nason, 1971; Burford et al., 1973; Goulty and Gilman, 1978; Goulty et al., 1978; Schulz et al., 1982). We have developed a relatively simple and low cost model of rod-type creepmeter (Fig. 5) in order to monitor the crustal deformation in the active fault zone. This creepmeter is generally 5–6 m long, and crosses through the active fault trace at a high angle from the fault strike. Depending on the instrument orientation and the geometry of the relative displacement in the fault, the fault slip will cause the distance between piers to either increase or decrease. In this study, the distances between the piers decrease because the Chihshang Fault continuously acted as a reverse fault, and also because the orientations of the creepmeters are parallel, or oblique at small angles relative to the displacement vectors of the fault creep (so that there is no configuration where the component of left-lateral strike–slip would result in lengthening along the creepmeter). Note, in a similar way, that the vertical component of fault displacement never suffices to induce lengthening.

In this study, we aim at elucidating the fault creep

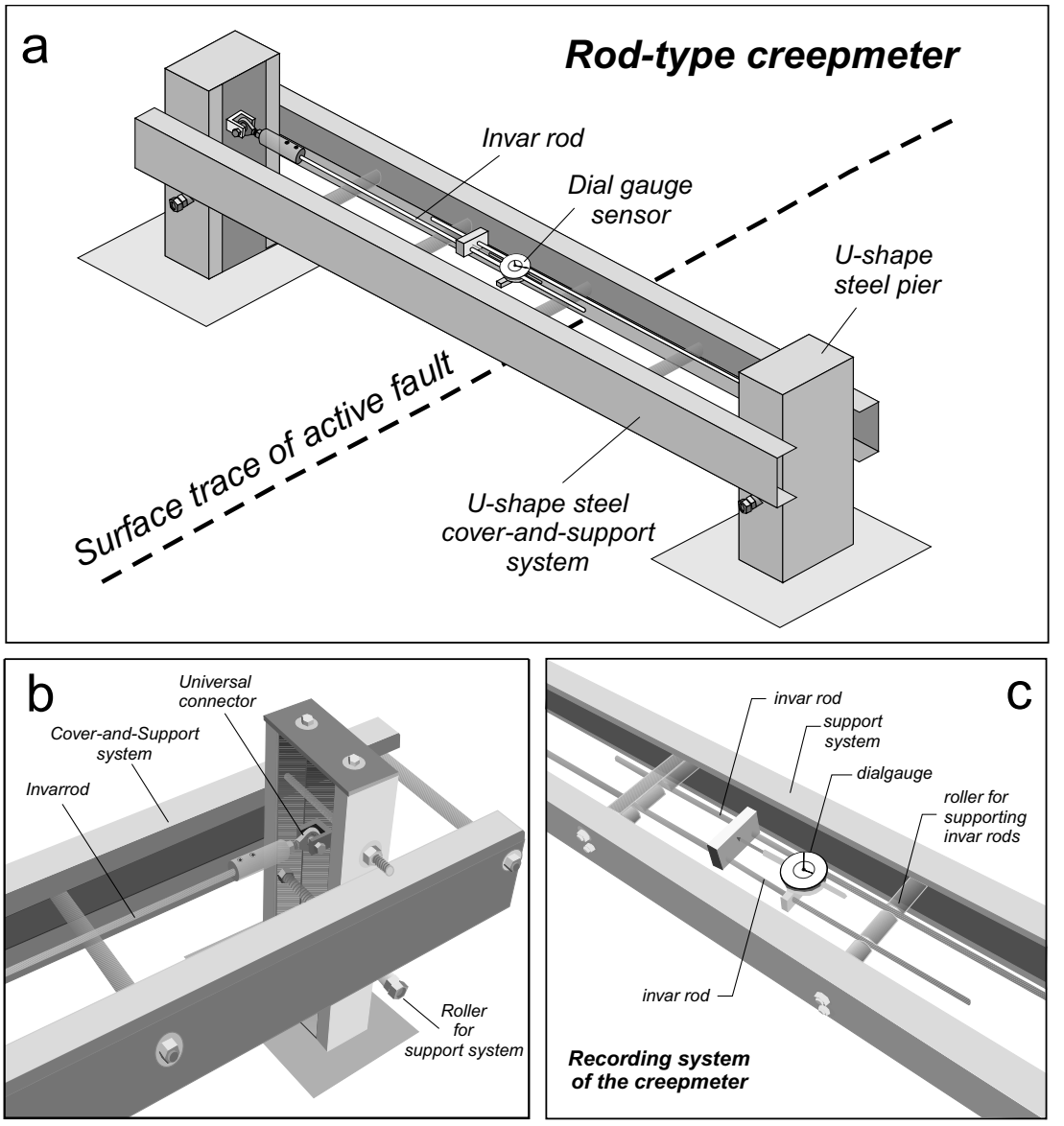


Fig. 5. (a) Schematic representation of the rod-type creepmeter across an active fault. The instrument measures the horizontal displacement between the anchored piers on the opposite sides of the active fault. (b) Details of the pier ends of the creepmeter. The invar rods are attached on each pier by a universal connector and are supported by the rollers fixed on a U-shaped steel cover-and-support system. (c) Details of the middle part of the creepmeter. The relative horizontal movement of two invar rods can be measured by a mechanical dial gauge sensor. The resolution of the dial gauge is up to 0.01 mm and ranging to 50 mm.

evolution in detail rather than reconstructing the complete 3D displacement vectors of the active fault. Therefore we installed a single creepmeter system crossing each surface fracture of the Chihshang active fault (a choice that precludes any complete determination of the 3D displacement based on consideration of the creepmeter data solely). By measuring the distance change between piers of the creepmeter, we can obtain the component of the fault creep movement along the direction of

the axis of the creepmeter. We point out, however, that a 3D displacement vector model of the slip of the Chihshang Fault had been established before, based on the geodetic information first (Lee and Angelier, 1993), and combining this information with in-site observation of displacements later (Angelier et al., 1997, 1999). Taking this earlier determination into additional account, it is possible to reconstruct the 3D evolution of the fault slip. The assumption underlying this reconstruction, however, would be that of a constant orientation of the slip vector through time. This assumption is reasonable at the annual scale because the orientation determinations mentioned above, from both the geodesy and the in-site observation, suggested that the average slip vector does not vary in orientation at the scale of about one year. But there is no datum available concerning its behaviour for short time spans. For this reason, we consider that at a time scale of weeks and less, it is better not to adopt this assumption of a constant orientation of slip, which is not supported by any available datum.

Our designed creepmeter is principally composed of two parallel invar rods (62% Fe, 36% Ni) which are attached to the anchored metal piers on each side across the active fault (Fig. 5). The invar rods are 3 to 4-m long and are 9.52 mm in diameter. The two piers are fixed on $60 \times 60$-cm$^2$ wide concrete basements buried in the ground and anchored with metal bars where the ground comprises soil. The concrete basements are, at most sites, built in 30 to 50-cm deep holes. The outside part of the creepmeter is a support-and-cover system, which suspends the invar rods and protects them from rains (Fig. 5a). The invar rods are connected to the piers by a universal joint, which is designed so as to leave them free to move along their axes (Fig. 5b). The support-and-cover system consists of two parallel U-shaped steel girders straddling on two piers. The recording system in the middle of the creepmeters comprises a dial-gauge sensor (Fig. 5c) with a basic unit marker of 0.01 mm, an instrumental resolution more than one order of magnitude better than the actual accuracy of our recording and observation, which averages 0.1 mm. The technique aspects of the instrumentation and the installation of the creepmeter can be referred to the more detailed descriptions by Lee et al. (2000).

Two aligned creepmeters (CHIH001 and CHIH002) were installed across the fault zone in the Tapo primary school (Fig. 6a), and three creepmeters were installed across three parallel branches of the fault zone in the Chinyuan village (CHIH003, CHIH004, and CHIH005).

At the Tapo primary school, the creepmeters are straddling the Chihshang active fault with the western pier installed on the flat alluvium deposits (belonging to the Longitudinal Valley) and the eastern pier installed on the inclined slope of the Lichi Mélange (belonging to the Coastal Range). These two creepmeters are aligned and have a common pier (Fig. 6a). The total displacement is given by the sum of the records of the two creepmeters. The fault structure at this site has been accurately known because of the excavation made during wall reconstruction in May 1997, as described by Chu et al. (1998). Although there is no doubt about this location of the active Chihshang Fault based on field studies, the displacement at Tapo may be influenced by both the well-known instability of the Lichi Mélange and the down slope sliding of the hill, east of the school (see discussion in Angelier et al., 1999). For this reason, the results obtained at this locality of the Tapo school must be considered with caution despite the spectacular aspect of fault displacement at this site. To this respect, in the forthcoming discussion, the interest of comparing the Tapo data and the Chinyuan data will be highlighted.

The creepmeters in the Chinyuan village were installed in three neighbouring places along a water channel, within a fault zone less than 100-m wide (Fig. 7). Contrary to the case of the Tapo school, the Chinyuan creepmeters (CHIH003, CHIH004, and CHIH005) were not implanted in the ground, but fixed in the concrete wall of the channel (Fig. 6b). This aspect is important, because of the rigidity of these walls that precludes local ground effects. As important is the morphology, which is nearly flat in and around this site so that no landsliding is expected.

Fig. 6. Photograph of rod-type creepmeter. (a) The creepmeters CHIH001 (the lower one) and CHIH002, having a common pier in the middle, across the active fault zone and aligned subperpendicular to the fault strike at the foot of rugged hills of the Coastal Range in the Tapo School. (b) The creepmeter CHIH004, straddling the surface fractures of the active fault, was installed on the wall of the water channel in the Chinyuan

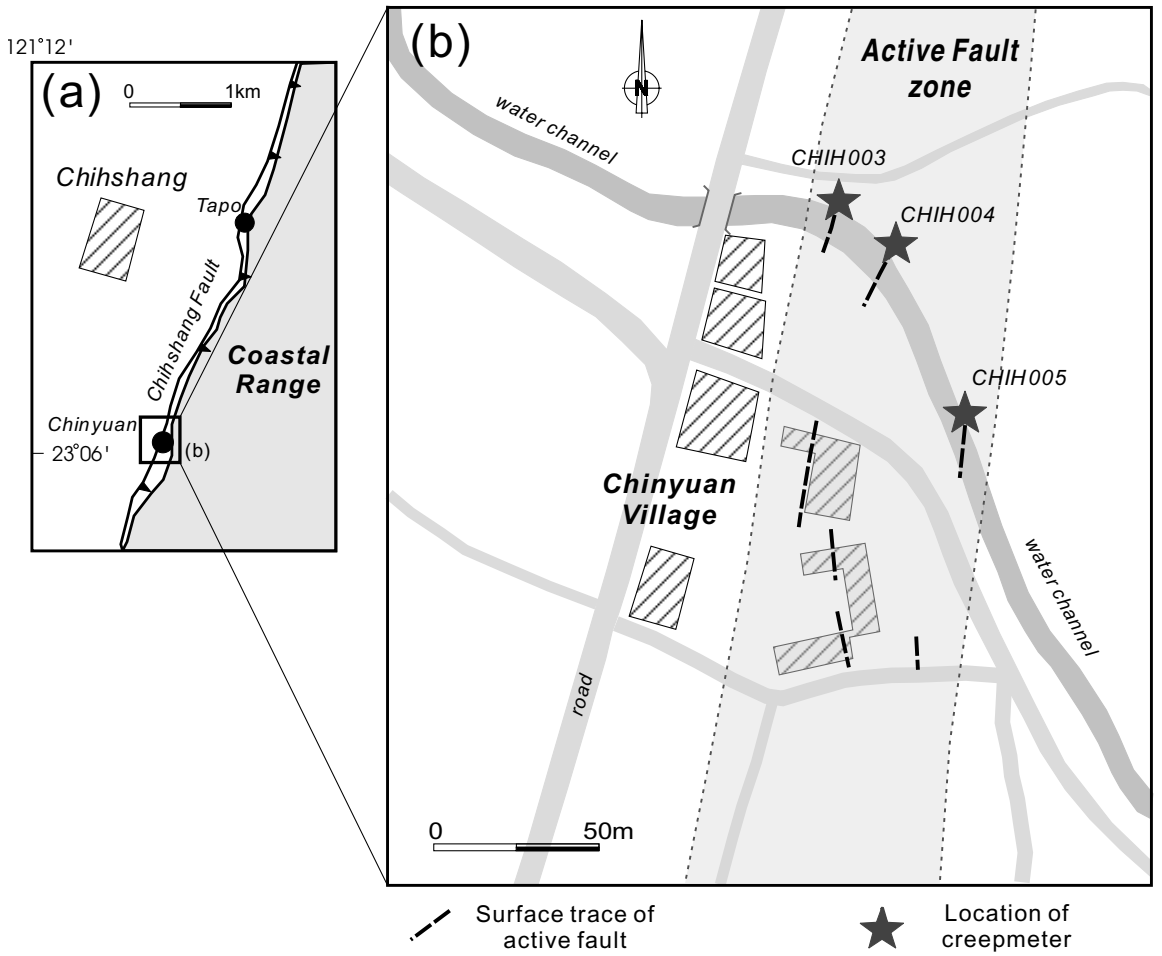


Fig. 7. Location of the creepmeters at the Chinyuan site. Three creepmeters were installed on the wall of the water channel where three surface ruptures of active fault have been observed within an about 100-m wide active fault zone.

For both these reasons, more confidence is given to the results from Chinyuan as far as the actual motion of the fault zone at depth is concerned. Geologically, all three Chinyuan creepmeters are situated on the flat recent alluvium deposits as revealed by the imagery of ground penetration radar (Chow et al., 2001). These three sites correspond to surface traces of the active faults, which have been investigated before (Chu et al., 1994; Angelier et al., 1997, 1999).

The orientations of the creepmeters are basically set to be parallel or at a small angle to trends of the general moving vectors (see Angelier et al., 1999) of the Chihshang fault, in order to measure the horizontal shortening by fault creep. The Tapo creepmeters trend N115°E. The three Chinyuan creepmeters, CHIH003, CHIH004, and CHIH005, trend N113°E, N156°E, and N164°E, respectively.

It is possible to calculate the actual horizontal components of the fault creep based on the combination of the measurements of the creepmeter, the relationship between the orientations of the fault and the creepmeter, and the slip vector of the fault. The latter two can be obtained by adopting the result of the previous studies (Lee and Angelier, 1993; Angelier et al., 1997, 1999). We can thus have the orientation of the Chihshang fault, that is a N18°E strike and an eastward dip of 45°. The slip vectors of the fault trend N156°E and plunge 32°S at Tapo; they trend N145°E

and plunge 27°S on average at Chinyuan. The relationship between the actual displacement vector of fault creep ($\Delta V$) and displacement of creepmeter ($\Delta S$) can thus expressed by Eq. (1):

$$\Delta S = \Delta V \cos(\theta_1 - \theta_2) \quad (1)$$

where $\theta_1$ is the azimuth of the orientation of the actual displacement vector and $\theta_2$ is the azimuth of the orientation of the creepmeter. We can thus obtain the strike-perpendicular component ($\Delta T$) and the strike-parallel component ($\Delta L$) of the actual displacement vector by using the azimuth of the fault ($\theta_3 = \text{N18°E}$) as shown by Eqs. (2) and (3), respectively:

$$\Delta T = \Delta V \cos[\theta_1 - (\theta_3 + 90)], \text{ that is,}$$

$$\Delta T = \Delta V \sin(\theta_1 - \theta_3) \quad (2)$$

$$\Delta T = \Delta S \sin(\theta_1 - \theta_3)/\cos(\theta_1 - \theta_2)$$

$$\Delta L = \Delta V \sin[\theta_1 - (\theta_3 + 90)], \text{ that is,}$$

$$\Delta L = \Delta V \cos(\theta_1 - \theta_3) \quad (3)$$

$$\Delta L = \Delta S \cos(\theta_1 - \theta_3)/\cos(\theta_1 - \theta_2)$$

## 4. Observation on creepmeters

### 4.1. Data collection and calibration

The five rod-type creepmeters were installed in late July 1998. The readings of the dial gauge sensors were taken daily for the first two months and then two to five times weekly. To check the reliability of readings, there were exchanges between observers in Tapo and Chinyuan at some periods. No difference was observed, indicating that full confidence could be given to the readings. The observation time was generally 4:00–6:00 p.m. (soon before sunset), in order to minimize the effects of temperature variation and to have regular time spacing in measurements.

Because the creepmeter is basically composed of metal materials and exposed under the sun, the effect of thermal expansion deserves consideration although a low thermal expansion material (the invar) had been adopted to build the rods of the creepmeters. In practice, the temperature effect has been evaluated by measuring the hourly changes during a time span of 30 h. The shortening amounts during a day are principally a function of the temperature variations. The corresponding data are plotted in Fig. 8, which well illustrates the daily fluctuation. During one day, with a temperature difference of 13.7°C (between 24.2 and 37.9°C), we obtained a variation in shortening of 0.71 mm for the creepmeter CHIH001. We then used the data of such measurements as the basis for temperature calibration. Under the reasonable assumption that during one day the fluctuation of shortening principally depends on the variations of the temperature, the thermal-elastic coefficients for each creepmeter can thus be calculated (Table 1). We have also carried out another 30-h run hourly measurements a year later to test the validity of this calibration. It shows very similar results of thermal-elastic coefficients for each creepmeter (Table 1). We thus consider this experimental determination more reliable than the theoretical evaluation based on the knowledge of invar properties.

### 4.2. Results of measurement of creepmeter

The results of the creepmeters for a year (August 1998 to July 1999) are illustrated by the shortening amounts versus time as Fig. 9 (at Tapo) and Fig. 10 (at Chinyuan).

Fig. 9 shows the displacement of the fault creep (shortening of creepmeter) with respect to time at the Tapo School, recorded by two aligned-connected creepmeters, CHIH001 and CHIH002. The plots reveal that the fault in general is continuously creeping. The total shortening (sum of the shortenings of two creepmeters) is 19.4 ± 0.3 mm for a year. The data indicate three distinct periods with different shortening rates: 29.1 ± 0.4 mm/year from August to November, 5.1 ± 0.5 mm/year from December to January, and 16.8 ± 0.2 from February to July. The creep rate periods show a general consistency with the rainfall data: the high creep rate period coincides with the high rainfall season and the low creep rate period coincides with the dry season. We will discuss the relationship between the rainfall and the fault creep in more detail in later section. The one-year shortening rate of 19.4 mm/year at the Tapo School is generally in a good agreement with the long-term shortening rate deduced from other estimates (Yu

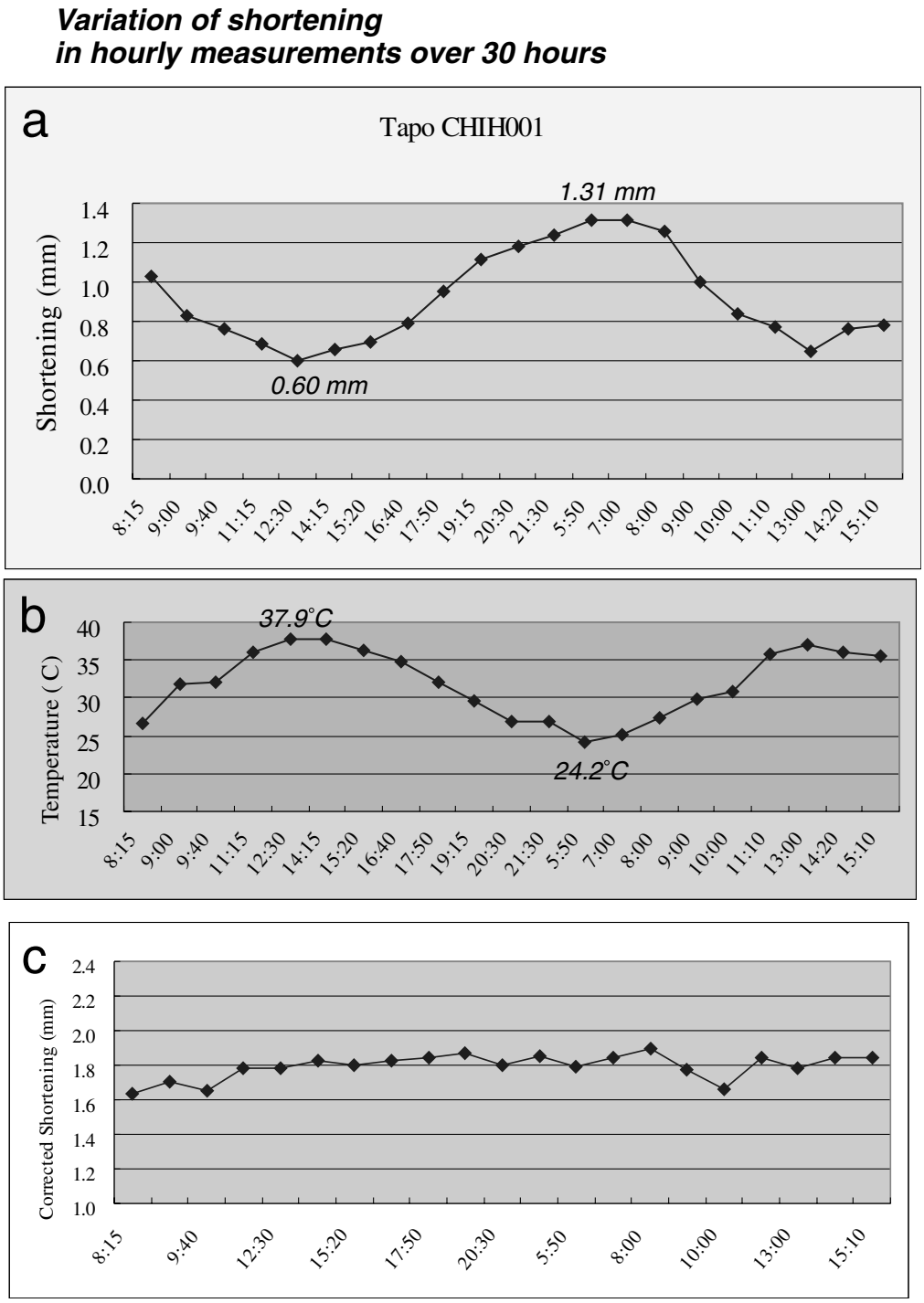


Fig. 8. Diagrams of hourly measurement during 30 h. (a) Shortening amount of creepmeter data versus time. (b) Temperature versus time. (c) Corrected shortening amount (based on thermal calibration in Table 1 versus time. The daily fluctuation is well illustrated in the plot. The variation indicates that the displacement (shortening amount) recorded by the creepmeter is strongly related to the thermal effect. The shortening amounts for each hourly measurement after corrected by thermal calibration show a good consistency.

Table 1
Parameters of the temperature effect and results of calculated temperature coefficients deduced from hourly measuring experiments during a time span of 30 h. The hourly measurements have been carried out twice: first on 27–28 July 1998, and second on 10–11 September 1999. The range of temperature represents the minimum and the maximum temperatures during 30 h. The difference of shortening represents the difference between the maximum and the minimum data readings during the same 30 h. The temperature coefficients for each creepmeter are calculated based on three parameters listed in the table. Note that the temperature coefficients for each creepmeter are similar between two different measurements (the temperature coefficient of invar rod used for creepmeter is $1.6 \times 10^{-6}$)

| Name of creepmeter | Range of temperature (°C) | Difference of shortening (mm) | Lengths of invar rods (mm) | Temperature coefficient (/°C) |
|---|---|---|---|---|
| *Date of measurement: 27–28 July 1998* | | | | |
| CHIH001 | 24.2–37.9 | 0.71 | 6020 | $8.6 \times 10^{-6}$ |
| CHIH002 | 24.3–37.2 | 0.52 | 7300 | $5.5 \times 10^{-6}$ |
| CHIH003 | 23.6–41.5 | 0.54 | 7310 | $4.1 \times 10^{-6}$ |
| CHIH004 | – | – | 5820 | – |
| CHIH005 | 24.4–39.3 | 0.755 | 7290 | $7.0 \times 10^{-6}$ |
| *Date of measurement: 10–11 September 1999* | | | | |
| CHIH001 | 21.4–35.9 | 0.677 | 6020 | $7.8 \times 10^{-6}$ |
| CHIH002 | 21.3–35.2 | 0.458 | 7300 | $4.5 \times 10^{-6}$ |
| CHIH003 | 21.2–36.6 | 0.421 | 7310 | $3.7 \times 10^{-6}$ |
| CHIH004 | 21.55–35.0 | 0.85 | 5820 | $10.8 \times 10^{-6}$ |
| CHIH005 | 21.5–35.5 | 0.67 | 7290 | $6.6 \times 10^{-6}$ |

and Liu, 1989; Lee and Angelier, 1993; Lee, 1994; Yu et al., 1997; Angelier et al., 1997).

There are different creep histories between the two creepmeters at Tapo (compare Fig. 9b and c). First, the lower creepmeter (CHIH001) located at the foot of the slope reveals a high-creep-rate period ($22.3 \pm 0.4$ mm/year in average) from August to mid-November (period A, the rainy reason), a low-creep-rate period ($5.6 \pm 0.3$ mm/year) from mid-November to March (period B, the dry season), and a moderate-creep-rate period ($12.5 \pm 0.5$ mm/year) from April to July (period C, the season with moderate rain). This suggests close correlation between fault creep and rainfall. In contrast, the displacement data of the upper creepmeter (CHIH002) are not compatible with a close relationship between fault creep and rainfall. These data revealed a low creep rate period ($6.2 \pm 0.1$ mm/year) from August to mid-February (period A′), a high creep rate period ($17.1 \pm 0.3$ mm/year) from mid-February to April (period B′), and a low creep rate period ($4.4 \pm 0.3$ mm/year) from May to July (period C′).

Fig. 10 illustrates the displacements of the fault creep with respect to time at Chinyuan, recorded by three creepmeters (CHIH003, CHIH004, and CHIH005), which distributed in a 100-m wide fault zone. The total shortening recorded by creepmeters is about $17.3 \pm 0.7$ mm for a year, which is similar to that measured at Tapo (19.4 mm/year). The plot shows three periods with different types of creep. From August 1998 to February 1999 (period D), the data of creepmeter reveal a very slow shortening rate of $0.6 \pm 0.4$ mm/year with a likely fluctuation. From March 1999, suddenly the fault moved with a high shortening rate of about $38.9 \pm 1.0$ mm/year (period E).

The creep behaviour in Chinyuan is more complex in comparison with that at Tapo School. For instance, the fluctuation during August to November still has no good explanation. One possibility is that the fault creeps may reflect the tidal fluctuation. The phenomenon of tidal fluctuation has been observed in other places from the measurements of strainmeters (e.g. King and Bilham, 1976). Concerning the period of high shortening rate starting in March 1999 (Fig. 10), one can note that the curves of shortening show several creep events with some abrupt jumps rather than smoothed movements. An interesting point is that generally each creep event affected all three creepmeters. In other words, the three branches of the Chihshang Fault at Chinyuan generally moved simultaneously during the creep events. Another point is that three creepmeters have similar creep

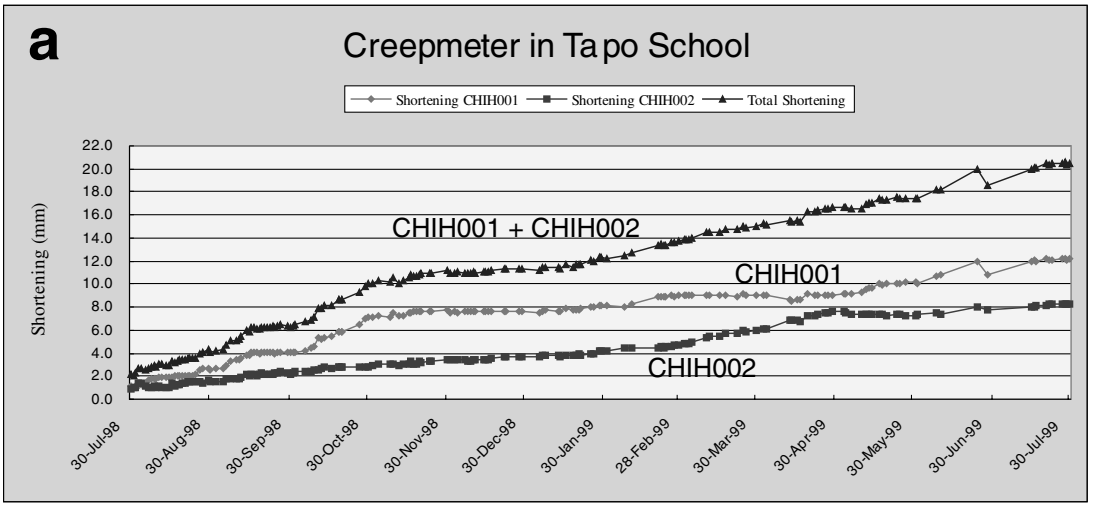
a
Creepmeter in Tapo School
Shortening CHIH001
Shortening CHIH002
Total Shortening
Shortening (mm)
CHIH001 + CHIH002
CHIH001
CHIH002
22.0
20.0
18.0
16.0
14.0
12.0
10.0
8.0
6.0
4.0
2.0
0.0
30-Jul-98
30-Aug-98
30-Sep-98
30-Oct-98
30-Nov-98
30-Dec-98
30-Jan-99
28-Feb-99
30-Mar-99
30-Apr-99
30-May-99
30-Jun-99
30-Jul-99

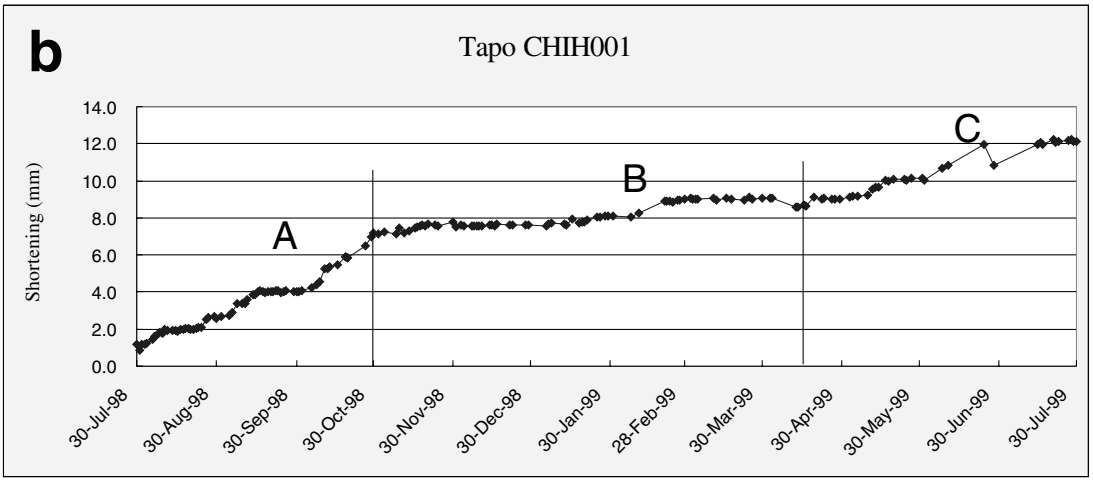
b
Tapo CHIH001
Shortening (mm)
A
B
C
14.0
12.0
10.0
8.0
6.0
4.0
2.0
0.0
30-Jul-98
30-Aug-98
30-Sep-98
30-Oct-98
30-Nov-98
30-Dec-98
30-Jan-99
28-Feb-99
30-Mar-99
30-Apr-99
30-May-99
30-Jun-99
30-Jul-99

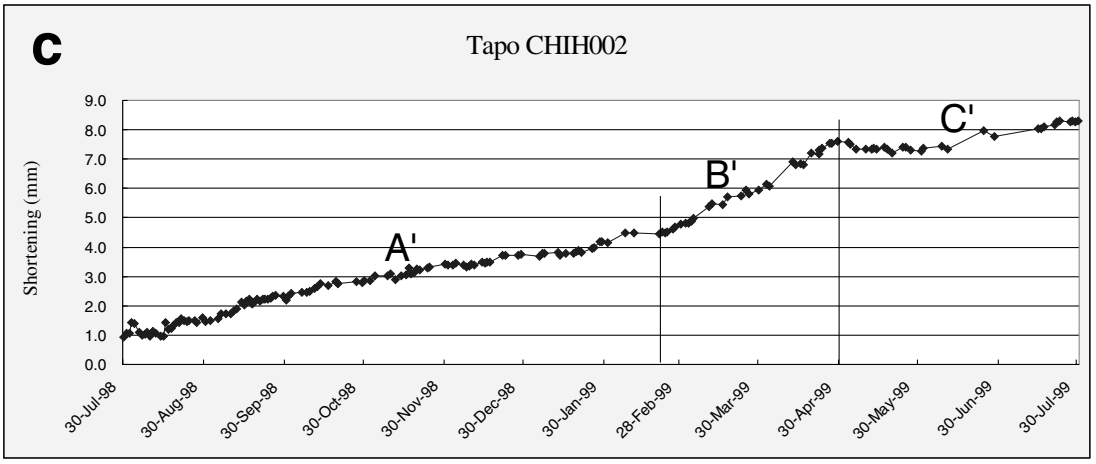
c
Tapo CHIH002
Shortening (mm)
A'
B'
C'
9.0
8.0
7.0
6.0
5.0
4.0
3.0
2.0
1.0
0.0
30-Jul-98
30-Aug-98
30-Sep-98
30-Oct-98
30-Nov-98
30-Dec-98
30-Jan-99
28-Feb-99
30-Mar-99
30-Apr-99
30-May-99
30-Jun-99
30-Jul-99

curves with very slow displacement rates for the first half of the period considered and with high rates for the second half. The creepmeter CHIH004 even shows lengthening during the first half. The reason why there occurred such limited extension before the rapid shortening remains unclear. One possible reason is that the concrete wall of the water channel may be slightly folded or tilted before slip occurred along the main fractures. Lacking of quantitative data concerning the vertical component of the creepmeters, it is difficult to evaluate the hypothesis.

### 4.3. Consistency with previous estimates

The one-year results of the creepmeters in the Chihshang active fault zone show an average horizontal shortening rate of about 17–19 mm/year in Tapo (19.4 mm/year) and Chinyuan (17.3 mm/year). These results are generally consistent with the previous estimates at various scales, including geodetic trilaterational measurements (Yu and Liu, 1989), GPS measurements (Yu et al., 1997), and the site investigations (Angelier et al., 1997, 1999). In particular, the site investigations and the measurements of creepmeters provide complementary estimates for the same surface fractures of the active fault. Fig. 11 summarizes previous estimates of the shortening at four sites along the Chihshang active Fault (Angelier et al., 1999). These outcrop observations include measurements of the displacements along the fault zone that have been carried out since 1990 and repeated annually (Fig. 11). The estimates of the fault slips showed a general consistency among the different sites with minor local variations, with an average velocity of horizontal shortening ranging between 22 and 29 mm/year (Angelier et al., 1997, 1999). Although the values obtained for one year from our creepmeter study fall in the same general figure, the velocity determined at Chinyuan is smaller than the average velocity. However, it should be noticed that the previous analyses also indicated relatively low local values of shortening at Chinyuan, so that at the local scale the fit is good. This probably results from the complicated distribution of fault slip at Chinyuan, where the fault deformation is not concentrated in a zone of few meters wide as it is at Tapo, but is distributed across a wider deformation zone. In Chinyuan, not only do three parallel branches of the fault accommodate the movement, but also some deformation occurs between these fractures and incipient in-sequence thrusting is even suspected downstream in the channel (Angelier et al., 1997). As a result, at Chinyuan, it is likely that the total deformation is not completely recorded from both the previous observations and our creepmeter data, which concern the discrete active fractures.

## 5. Discussions

The measured deformation at the creepmeter can result from different sources: tectonic stress, soil creep, earth tides, human activity, and atmospheric factors (e.g. rainfall, temperature, air pressure, etc.). The creepmeters have been installed across the surface fractures of the active fault which has been moving continuously during the last few years. Therefore, we can conclude that the measured deformation of the creepmeters in the Chihshang area is principally related to tectonic movement. However, other factors, such as rainfall and temperature, also play important roles, which can not be ignored. In this section, we will discuss the factors which may affect the creepmeter measurements.

### 5.1. Seasonal variation at Tapo school site

The shortening rates deduced from the creepmeters in the Tapo elementary school reveal a remarkable seasonal variation. The recording period can be divided into three sub-periods: the first from August to November 1998 (Period $A''$), the second from December 1998 to January 1999 (Period $B''$), and the third from February to July 1999 (Period $C''$).

Fig. 9. Data of the creepmeters at Tapo elementary school. Two creepmeters, CHIH001 (diamond) and CHIH002 (square), are connected together to measure the displacement in a 10–15-m-wide active fault zone situated at the foot of a small hill. The sum of the data of two creepmeters represents the total shortening amount. A, B, C for creepmeter CHIH001 and $A'$, $B'$, $C'$ for creepmeter CHIH002 represent periods of different shortening rates (see text for details).

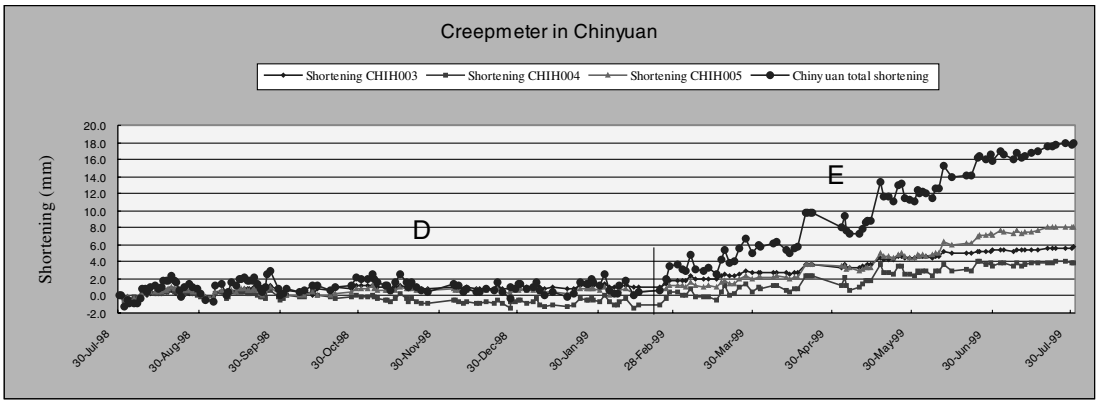
Creepmeter in Chinyuan
Shortening CHIH003
Shortening CHIH004
Shortening CHIH005
Chinyuan total shortening
Shortening (mm)
D
E
30-Jul-98
30-Aug-98
30-Sep-98
30-Oct-98
30-Nov-98
30-Dec-98
30-Jan-99
28-Feb-99
30-Mar-99
30-Apr-99
30-May-99
30-Jun-99
30-Jul-99

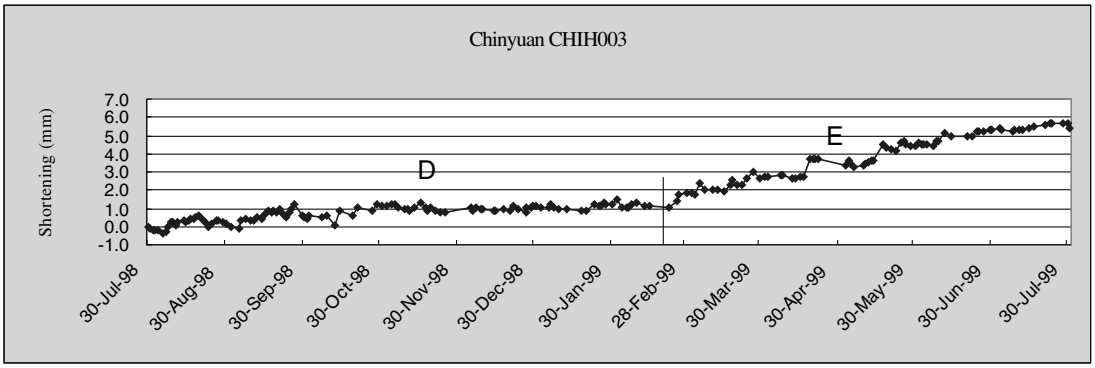
Chinyuan CHIH003
Shortening (mm)
D
E
30-Jul-98
30-Aug-98
30-Sep-98
30-Oct-98
30-Nov-98
30-Dec-98
30-Jan-99
28-Feb-99
30-Mar-99
30-Apr-99
30-May-99
30-Jun-99
30-Jul-99

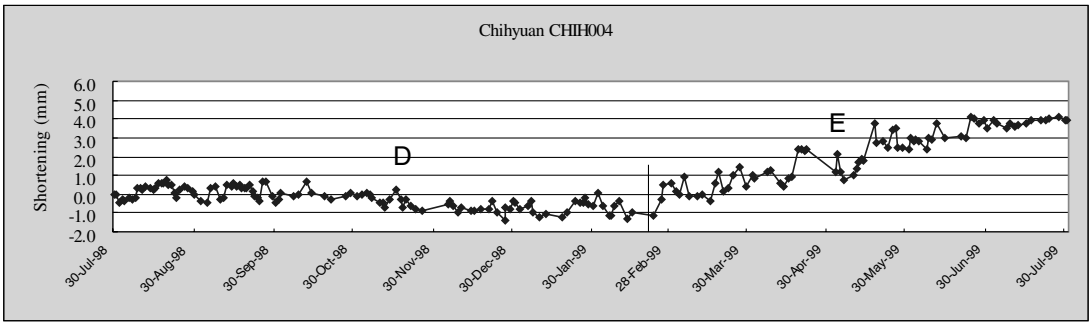
Chihyuan CHIH004
Shortening (mm)
D
E
30-Jul-98
30-Aug-98
30-Sep-98
30-Oct-98
30-Nov-98
30-Dec-98
30-Jan-99
28-Feb-99
30-Mar-99
30-Apr-99
30-May-99
30-Jun-99
30-Jul-99

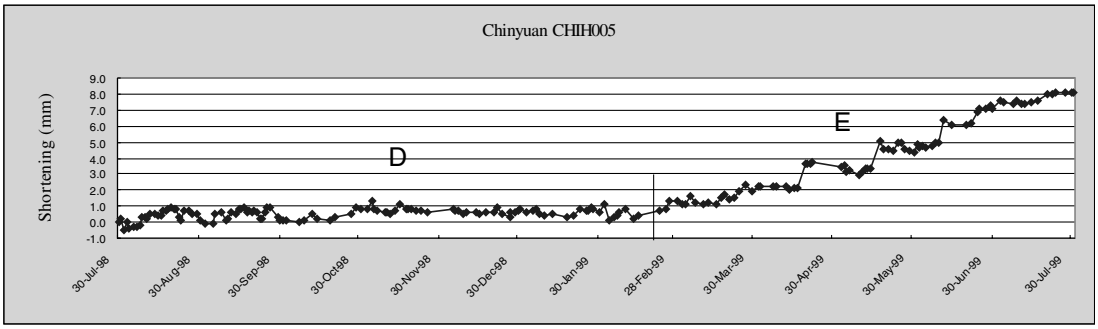
Chinyuan CHIH005
Shortening (mm)
D
E
30-Jul-98
30-Aug-98
30-Sep-98
30-Oct-98
30-Nov-98
30-Dec-98
30-Jan-99
28-Feb-99
30-Mar-99
30-Apr-99
30-May-99
30-Jun-99
30-Jul-99

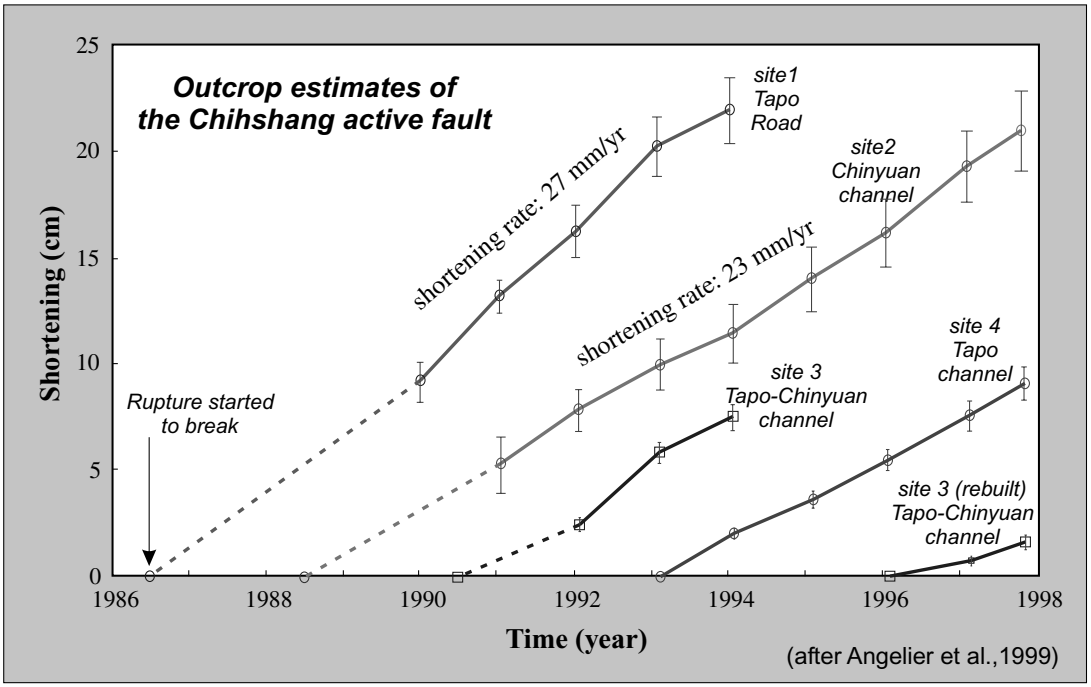


Fig. 11. Displacements of the active Chihshang Fault from outcrop estimates (after Angelier et al., 1999). Four sites from Tapo to Chinyuan allow reconstructing the displacements and shortening rate of the Chihshang fault.

One possible cause for these changes of shortening rate can be attributed to the water (meteorological) effect. The rainfall data have been compared with the shortening rate of the creepmeters as illustrated in Fig. 12. The Period A″ corresponds to the wet season, the Period B″ corresponds to the dry season, and the Period C″ corresponds to the season with moderate rainfall. There is a simple possible interpretation of this seasonal variation. During the wet season, the fault was more active at the surface because the water acted as a lubricant along the fault surface, thus making movement easier because of the lesser friction. During the dry season, the coefficient of friction increased so that the uppermost part of the fault surface became temporarily locked. This interpretation implies that in the uppermost section the material around the fault zones undergoes alternating periods of stress accumulation (during the dry season) and release (during the wet season). These variations are too small to induce noticeable earthquakes, because taking the shortening velocity into account the locking periods are not long enough to allow large stress accumulation. It would be of interest, however, to survey the very shallow microearthquake activity in the area in order to detect its possible periodicity.

The recent in-site investigations also indicate a seemingly seasonal variation of the fault creep. We acknowledge, on the one hand, that our interpretation is based on one year only (August 1998 to July 1999) of creepmeter recording, which of course is not enough to reliably establish a seasonal variation. On the other hand, the in-site observations that were carried out twice a year (in February and November) during the last two years revealed intriguing contrasts in average velocities that were fitting very well the model of

Fig. 10. Data of the creepmeters in Chinyuan. Three creepmeters, CHIH003 (diamond), CHIH004 (square), and CHIH005 (triangle), are located individually at the surface traces in a 100-m wide active fault zone. D and E represent periods of different shortening rates (see text for details).

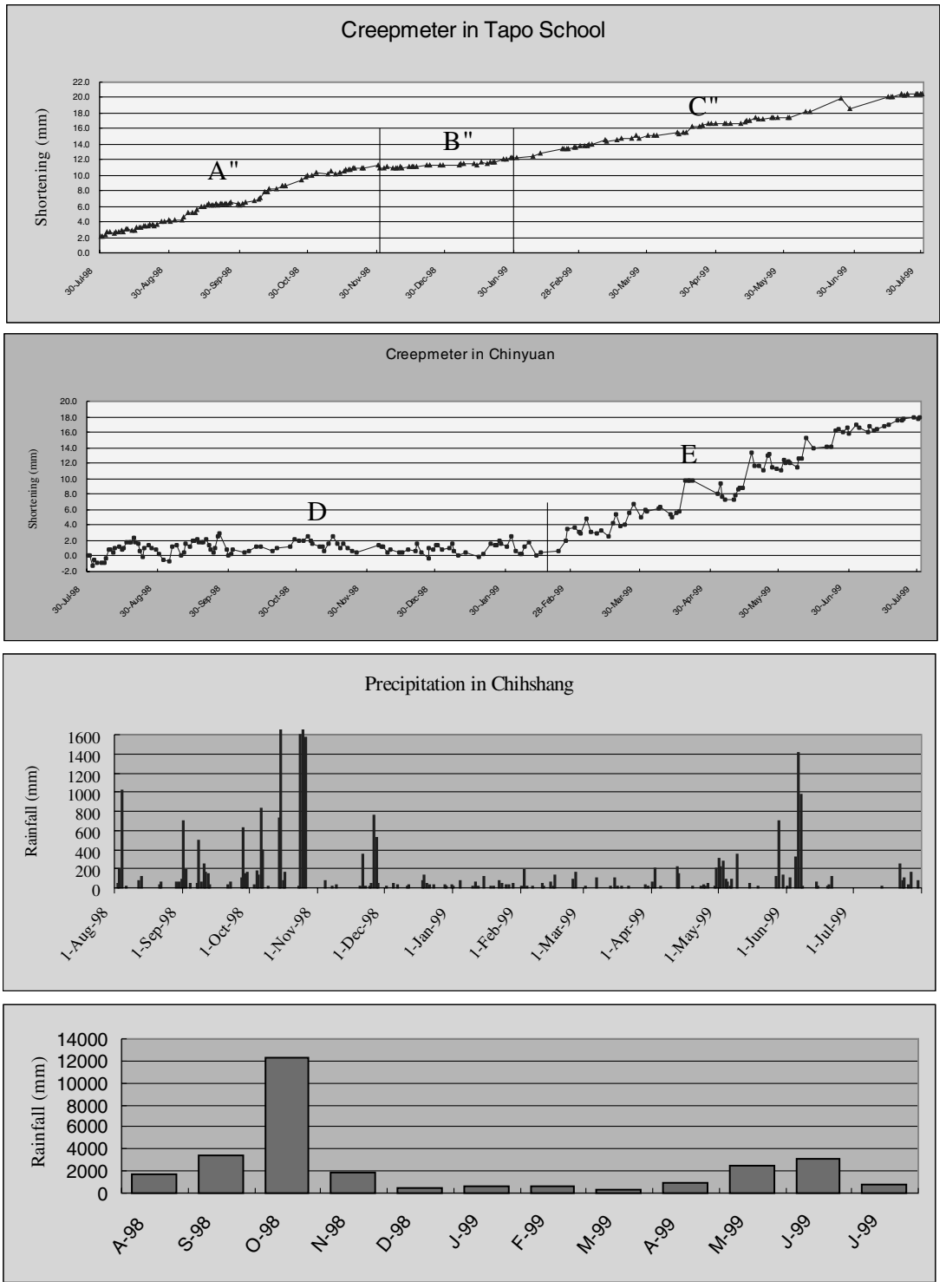


Fig. 12. Comparison between the movements of fault creep and rainfall in the active Chihshang Fault zone. The upper two plots show the shortening of the creepmeters with respect to time in Tapo and Chinyuan. The lower two plots show the rainfall data.

seasonal variation discussed above (that is, the average displacement velocity was much smaller from November to February than for February to November). Such changes had never been detected before, because previous surveys were made once a year (Angelier et al., 1997, 1999). This earlier observation brings some additional support to our interpretation, which however, needs more data to be validated.

It is common that the near-surface deformation is correlated with rainfall. The mechanisms connecting rainfall to related deformation are complex and likely to be nonlinear (Agnew, 1986). These mechanisms remain still unclear, although a physical elasticity theory has been proposed (Dal Moro and Zadro, 1998). Shallow installations of creepmeters are usually affected by the meteorological effects, which arise from local soil motions caused by wetting and drying (Agnew, 1986).

### 5.2. Complex variation at Chinyuan site

The shortening rates of the creepmeters at the Chinyuan site show a relatively complex creep history (Fig. 10). The one-year record of fault creep can be divided into two sub-periods: the first from August 1998 to February 1999 (Period D) and the second from February to July 1999 (Period E). In the Period D, the shortening rate was very slow and fluctuations can be clearly observed especially from August to November. On the contrary, the Period E (from February to July 1999) shows numerous activities of creep with high shortening rates. By comparison with the rainfall data (Fig. 12), we can find that the variations in shortening rate at Chinyuan in general are not very consistent with the precipitation history. Four principal factors may have played important roles in the processes of the fault creep, including thermal effect of the wall of the water channel, earth tidal effect, water table in the nearby rice field, and rainfall.

The shortening rates of the creepmeters in the Chinyuan channel seemingly show a monthly fluctuation during the first two months. This tendency of monthly fluctuation is reflected by all three independent creepmeters, and thus can hardly be attributed to particular site effect. We consequently tend to interpret this as an earth tidal effect.

The results of creepmeters show that the creep history in Chinyuan is more complex than that in Tapo (compare Fig. 9 and Fig. 10). For example, monthly fluctuation occurred at the beginning and many abrupt jumps of creep can be observed. The fact that three sites generally move simultaneously suggests that the creeps should be caused by natural rather than human interference. The reason why the creep movements in Chinyuan were irregular still remains unclear. The other most important factor rather than tectonics at the Chinyuan site could be the effect of water, because the creepmeters in Chinyuan are situated close to a rice field which was filled with water in some periods. The water content of the near-surface soils, which was influenced by the wet-and-dry periods of the rice field, would have affected the creep rate of the fault to some extent.

### 5.3. Variations between Tapo and Chinyuan

The shortening in the Tapo primary school reveals a different history of creep and a larger shortening than that in the Chinyuan water channel. Based on the geodetic analysis (Yu and Liu, 1989; Lee and Angelier, 1993) and the site investigation (Lee, 1994; Angelier et al., 1997, 1999), they are the same segment of the active Chihshang Fault in Tapo and Chinyuan with a consistent shortening rate during the last 15 years. A first difference, as discussed in an earlier section of this paper, lies in the distribution of shortening across a wider shear zone in Chinyuan, so that part of the displacement may not be recorded by our three creepmeters (although they capture most of it). A second difference lies in the different context at Tapo and Chinyuan, as far as the geology and the morphology are concerned. Whereas the site of Chinyuan is located within the faulted alluvial deposits in a flat field, the site of Tapo is located at the foot of a small hill, along the fault boundary between the Lichi Mélange and the Quaternary alluvial deposits. This difference may explain the difference in creep history between the two sites. For instance, the high shortening rate in the Tapo suggests that there may be some combined effects of the shortening across the active fault and the gravitational sliding of the hill slope. Other possibilities, such as deformation occurring elsewhere than in the zones of the creepmeters for the low shortening rate in Chinyuan, cannot be excluded. In fact, recent results of GPS measurements (Yu et al., 1997) show a larger displacement

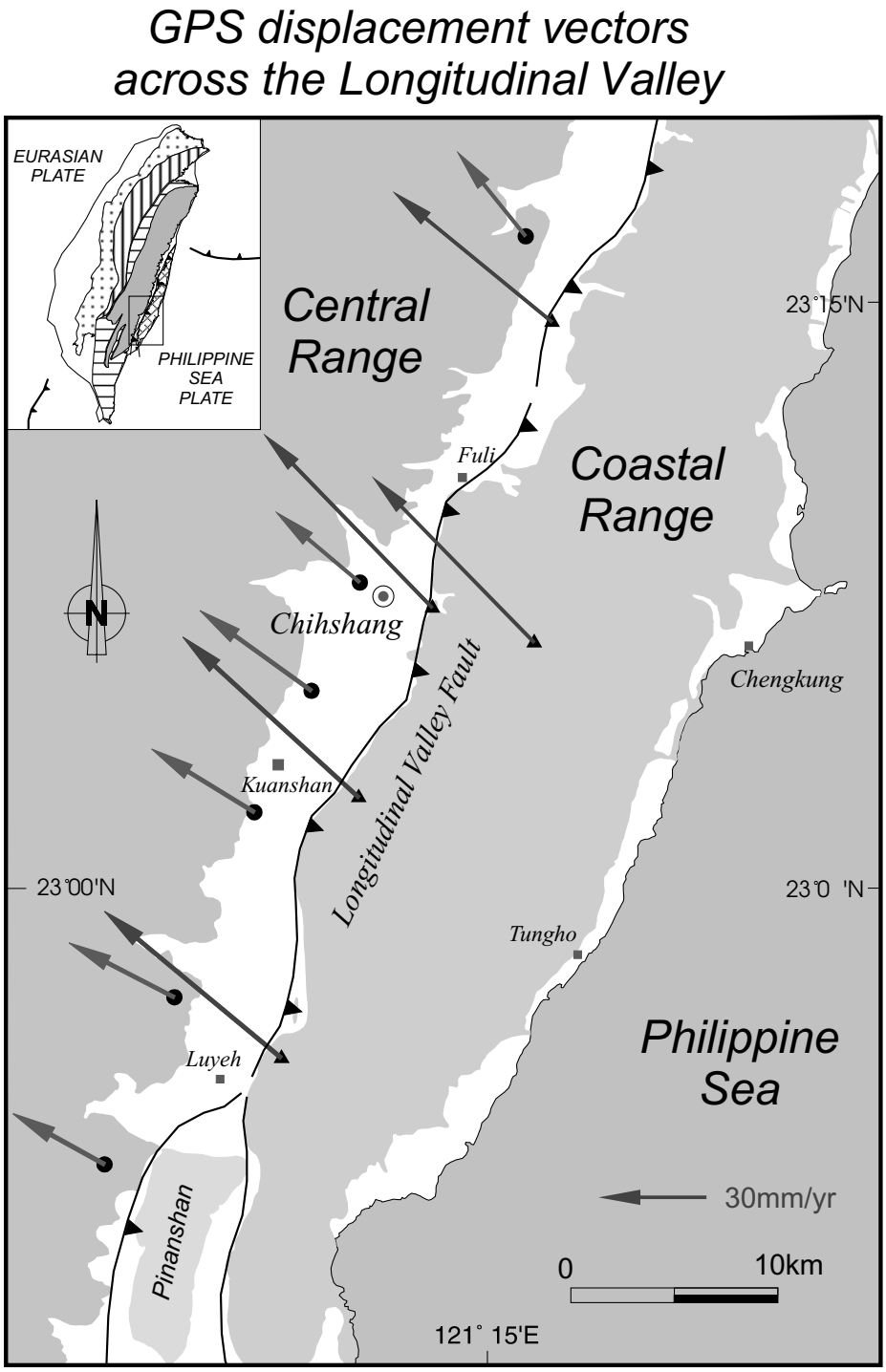


Fig. 13. Displacement vectors deduced from GPS measurements across the southern Longitudinal Valley. Five stations near the valley in the Coastal Range (triangles) and six stations near the valley in the Central Range (circles) have been plot. Each vector represents the annual displacement vectors (1990–1995) for each station relative to the Paisha station situated in Taiwan Strait.

(~30 mm/year) across the Longitudinal Valley. This also implies that there may exist other deformation outside of the zone of creepmeters. The next section will give more details.

### 5.4. Comparison with displacement vectors from GPS measurement

Several previous studies, including the analysis of the geodetic trilateration network and the geological surface investigation, indicate that the active deformation across the 5–10 km wide Longitudinal Valley is concentrated in the Chihshang active fault zone. The displacements of the fault creep from creepmeters in this paper are measured within this 30–100-m wide active fault zone. Still, deformation may occur in other places rather than the Chihshang Fault zone across the Longitudinal Valley. Recent GPS measurements provide a complementary data to compare with the outcrop creepmeter measurements of active fault creep.

Fig. 13 shows the displacement vectors deduced from the GPS measurements (Yu et al., 1997) across the southern Longitudinal Valley around the Chihshang area. Each vector represents the average annual displacement (1990–1995) for each station relative to the base station Paisha island (see Yu et al., 1997) situated in the stable continental margin of Taiwan Strait. In this figure, five GPS stations in the Coastal Range and six stations in the Central Range have been chosen in order to compare the displacements on the two sides of the Longitudinal Valley. The average of the five vectors in the Coastal Range, 62.9 mm/year in the direction of N313°E, is adopted as the representative displacement vector of the Coastal Range. The average of the six vectors in the Central Range, 32.6 mm/year in the direction of N306°E, is adopted as the representative displacement vector of the Central Range. The displacement vector across the Longitudinal Valley can thus be obtained as 31 mm/year in the direction of N320°E.

The recent 1990–1995 annual horizontal displacement of the Coastal Range related to the Central Range deduced from GPS measurement as revealed above (31 mm/year) is generally larger than other estimates focused on the Chihshang active fault (about 20 mm/year) including this study. One can thus expect that there exists deformation (about one third of the total shortening across the Longitudinal Valley area) in other places than the observed area of the Chihshang active fault zone.

## 6. Conclusions

(1) We have developed a rod-type creepmeter straddling the surface rupture of active fault in order to continuously monitor the movement of the active fault. The creepmeters are each composed of two invar alloy rods, which attached to the firmly anchored piers on each end.

(2) Five creepmeters have been installed at two sites in the Chihshang Fault zone, which is an active segment of the LVF, the main present-day suture between the Philippine and Eurasian plates in eastern Taiwan.

(3) One-year results (from August 1998 to July 1999) of creepmeter measurements in the Chihshang Fault zone show a horizontal shortening of $19.4 \pm 0.3$ mm and $17.3 \pm 0.7$ mm at Tapo and Chinyuan sites, respectively. These annual shortening rates are consistent with other previous estimates from geodetic measurements and geological in-site observation.

(4) The creep rate of active fault at Tapo site, especially for the creepmeter CHIH001, is closely correlated with the precipitation: a relatively high creep rate of about 29 mm/year during the wet season from August to November, a low creep rate of 5 mm/year during the dry season from December to January, and a moderate creep rate of 17 mm/year during the transition period from February to July.

(5) The creep behaviour of active fault at Chinyuan site is more complex and irregular. The reason still remains unclear. The possible factors causing a complex variation at Chinyuan may include the thermal effect of the concrete basement, earth tidal effect, water table in the nearby rice field, rainfall, etc.

(6) Based on comparison between the GPS survey at the scale of the Longitudinal Valley and the local creepmeter measurements, one infers that there exists other deformation than that recorded by our creepmeters in the active Chihshang Fault zone.

## Acknowledgements

This study was done under the France–Taiwan cooperation framework (Institut Français à Taipei and the National Science Council of Taiwan). This work

was also supported by the Institute of Earth Sciences, Academia Sinica, Central Geological Survey, National Taiwan University, and National Science Council grants NSC88-2116-M047-004. Helpful reviews by K. Berryman, D. Darby, S.B. Yu, and S. Dominguez greatly improved the manuscript. We gratefully thank the former principal of Tapo elementary school Shern-Hsiung Chang, Mr Guo-jang Jiang, Mr Yin-Peng Tsao and Miss Mei-Chi Lu, who provided numerous local facilities and help. This is a contribution of the Institute of Earth Sciences, Academia Sinica.

## References

Agnew, D.C., 1986. Strainmeters and tiltmeters. Rev. Geophys. 24 (3), 579–624.

Angelier, J., Chu, H.T., Lee, J.C., 1997. Shear concentration in a collision zone: kinematics of the active Chihshang Fault, Longitudinal Valley, eastern Taiwan. Tectonophysics 274, 117–144.

Angelier, J., Chu, H.T., Lee, J.C., Hu, J.C., 1999. Active faulting and earthquake risk: the Chihshang Fault case, Taiwan. J. Geodyn. 29, 151–185.

Barrier, E., Chu, H.T., 1984. Field trip guide to the Longitudinal Valley and the Coastal Range in eastern Taiwan. Sino-French Colloquium, pp. 27–49.

Barrier, E., Angelier, J., 1986. Active collision in Eastern Taiwan: the Coastal Range. Tectonophysics 125, 39–72.

Burford, R.O., Allen, S.S., Lamson, R.J., Goodreau, D.D., 1973. Accelerated fault creep along the central San Andreas fault after moderate earthquakes during 1971–1972. In: Nur, R.L.K.a.A. (Ed.), Proceedings of the Conference on Tectonic Problems of the San Andreas Fault System. Stanford Univ. Publ. Geol. Sci., pp. 268–274.

Cheng, S.N., Yeh, Y.T., Yu, M.S., 1996. The 1951 Taitung earthquake in Taiwan. J. Geol. Soc. China 39 (3), 267–285.

Chow, J., Angelier, J., Hua, J.J., Lee, J.C., Sun, R., 2001. Paleoseismic event and active faulting: a study of ground penetration radar and high resolution seismic reflection of the Chihshang fault, eastern Taiwan. Tectonophysics 333 (1–2).

Chu, H.T., Lee, J.C., Angelier, J., 1994. Non-seismic rupture of the Tapo and the Chinyuan area on the southern segment of the Huatung Longitudinal Valley Fault, Eastern Taiwan. Annual meeting of Soc. Geol. China, Taipei, pp. 1–5.

Chu, H.T., Angelier, J., Lee, J.C., 1998. Field trip guide to the active Chihshang Fault: a non-seismic rupture of the Tapo and the Chinyuan area on the southern segment of the Longitudinal Valley Fault, eastern Taiwan. In: Lee, H.T.C.a.J.C. (Ed.), Field Guidebook of Western Pacific Geophysics Meeting, Taipei, pp. 1–11.

Dal Moro, G., Zadro, M., 1998. Subsurface deformations induced by rainfall and atmospheric pressure: tilt/strain measurements in the NE-Italy seismic area. Earth Planet. Sci. Lett. 164, 193–203.

Goulty, N.R., et al., 1978. Large creep events on the Imperial fault, California. Bull. Seismol. Soc. Am. 68, 517–522.

Goulty, N.R., Gilman, R., 1978. Repeated creep events in the San Andreas fault near Parkfield, California, recorded by a strainmeter array. J. Geophys. Res. 83, 5415–5419.

Hsu, T.L., 1955. The earthquakes of Taiwan. Q. J. Bank of Taiwan 7, 39–63 (in Chinese).

Hsu, T.L., 1956. Geology of the Coastal Range, Eastern Taiwan. Bull. Geol. Surv. Taiwan 9, 39–64.

Hsu, T.L., 1962. Recent faulting in the Longitudinal Valley of eastern Taiwan. Mem. Geol. Soc. China 1, 95–102.

Hsu, T.L., 1976. Neotectonics of the Longitudinal Valley, Eastern Taiwan. Bull. Geol. Surv. Taiwan 25, 43–53.

King, G., Bilham, R., 1976. A geophysical wire strainmeter. Bull. Seismol. Soc. Am 66 (6), 2039–2047.

Lee, J.C., Angelier, J., 1993. Location of active deformation and geodetic data analyses: an example of the Longitudinal Valley Fault, Taiwan. Bull. Soc. Geol. France 164 (4), 533–570.

Lee, J.C., 1994. Structure et déformation active d'un orogène: Taiwan. Mem. Sc. Terre, 94-17 Thesis, Universite Pierre et Marie Curie, Paris, 281 pp.

Lee, J.C., Angelier, J., Chu, H.T., Yu, S.B., Hu, J.C., 1998. Plate-boundary strain partitioning along the sinistral collision suture of the Philippine and Eurasian plates: analysis of geodetic data and geological observation in southeastern Taiwan. Tectonics 17 (6), 859–871.

Lee, J.C., Jeng, F.S., Chu, H.T., Angelier, J., Hu, J.C., 2000. A rod-type creepmeter for measurement of displacement in active fault zone. Earth Planets Space 52, 321–328.

Nason, R.D., 1971. Measurements and theory of fault creep slippage in central California. Bull. R. Soc. N. Z. 9, 181–187.

Page, B.M., Suppe, J., 1981. The Pliocene Lichi melange of Taiwan; its plate-tectonic and olistostromal origin. Am. J. Sci. 281 (3), 193–227.

Schulz, S.S., Mavko, G.M., Burford, R.O., Stuart, W.D., 1982. Long-term fault creep observations in central California. J. Geophys. Res. 87 (B8), 6977–6982.

Smith, S.W., Wyss, M., 1968. Displacement on the San Andreas fault subsequent to the 1966 Parkfield earthquake. Bull. Seismol. Soc. Am 58, 1955–1973.

Stanley, R.S., Hill, L.B., Chang, H.C., Hu, H.N., 1981. A transect through the metamorphic core of the central mountains, southern Taiwan. Mem. Geol. Soc. China 4, 443–473.

Teng, L.S., Wang, Y., 1981. Island arc system of the Coastal Range, eastern Taiwan. Proc. Geol. Soc. China 24, 99–112.

Tsai, Y.B., 1986. Seismotectonics of Taiwan. Tectonophysics 125, 17–38.

TWB, 1952. Earthquake Report 1951 (in Chinese). Taiwan Weather Bureau, Taipei.

Yu, S.B., Tsai, Y.B., 1982. A study of microseismicity and crustal deformation of the Kuangfu-Fuli area in eastern Taiwan. Bull. Inst. Earth Sci. Accad. Sinica 2, 1–18.

Yu, S.B., Liu, C.C., 1989. Fault creep on the central segment of the longitudinal valley fault, Eastern Taiwan. Proc. Geol. Soc. China 32 (3), 209–231.

Yu, S.B., Jackson, D.D., Yu, G.K., Liu, C.C., 1990. Dislocation model for crustal deformation in the Longitudinal Valley area, eastern Taiwan. Tectonophysics 183, 97–109.

Yu, S.B., Chen, H.Y., Kuo, L.C., 1997. Velocity field of GPS stations in the Taiwan area. Tectonophysics 274, 41–59.